Electrochemistry Communications 121 (2020) 106865

Contents lists available at ScienceDirect

Electrochemistry Communications

journal homepage: www.elsevier.com/locate/elecom

On the reaction rate distribution in porous electrodes

Zhiqiang Chen [a,b,1], Dmitri L. Danilov [a,b,1], Rüdiger-A. Eichel [b,c], Peter H.L. Notten [a,b,d,*]

[a] Eindhoven University of Technology, Eindhoven 5600 MB, the Netherlands
[b] Fundamental Electrochemistry (IEK-9), Forschungszentrum Jülich, D-52425, Germany
[c] RWTH Aachen University, D-52074 Aachen, Germany
[d] University of Technology Sydney, Broadway, Sydney, NSW 2007, Australia

ARTICLE INFO

Keywords:
Reaction rate distribution
Effective electronic conductivity
Effective ionic conductivity
Porous electrode

ABSTRACT

Reaction rate distribution across porous electrodes in Li-ion battery applications largely determines the overall battery performance. In the present work, expressions for the reaction rate distribution across porous electrodes are analytically derived and analyzed for small current and short time applications. The dependency on the effective ionic and electronic conductivities is systematically investigated and discussed. It is found that in the case of equal effective electronic and ionic conductivities, the reaction rate distribution is symmetric around the electrode mid-point. Small conductivities induce the charge-transfer reaction to preferentially occur at the interface of the current collector and separator, while high conductivities make the reaction rate distribution uniform across the electrode thickness. In the case of unequal conductivities, a decrease in the effective electronic conductivity shifts the reaction rate distribution towards the electrode/current collector interface. In contrast, a decrease in the effective ionic conductivity shifts the reaction rate distribution towards the electrode/separator interface. It is also found that the reaction rate distribution shows saturating behavior when the effective electronic or ionic conductivity grows infinitely. A further increase in the effective ionic or electronic conductivity does not lead to any further reaction rate distribution changes.

1. Introduction

Lithium-ion batteries (LIB) with high energy density are highly demanded in our present-day society. Various efforts have been made to increase the energy density of these batteries [1], such as increasing the materials tap density [2,3], electrode thickness [4,5], *etc.* One of the drawbacks of increasing the thickness or tap density is the limited use of active materials inside porous electrodes at a fixed (dis)charging window [6,7]. Consequently, the non-uniform (de)lithiation processes across the electrode thickness play an important role.

The (de)lithiation reaction rate distribution across the porous electrode thickness is, in general, not uniform due to many factors [8]. Some experiments have been designed to display the non-uniformity of the charge-transfer reaction during operations [9–14]. The effective ionic conductivity of the electrolyte and the effective electronic conductivity of the electrode are proven to be highly responsible for these reaction rate distributions [15,16]. Although these experimental results are promising, they need a unique design of equipment and careful experiment planning. Moreover, it is not easy to discern the reaction rate or current distribution across the porous electrode thickness especially at short time scales. Using mathematical models are, therefore, highly advantageous as these offer a reliable way to analyze these properties by determining the physical and chemical parameters of LIB.

Porous electrode models [17–25] have been successfully adopted to analyze the reaction rate distribution in rechargeable batteries. The Tafel approximation [17] was applied to the Butler-Volmer equation at high overpotentials to derive analytical equations for the reaction rate or current distribution without considering any concentration gradients in the electrolyte and electrodes. On the other hand, a linear approximation has been applied to the Butler-Volmer equation at low overpotentials, and a general solution was presented at short time intervals as an inverse Laplace transform and asymptotical expression [19]. Four dimensionless ratios [17–19,23] were proposed to determine the reaction rate distribution across porous electrodes, namely the dimensionless current density, the dimensionless exchange current, the ratio of the charge-transfer coefficient, and the ratio of effective conductivities. Three of these four dimensionless ratios are involved in the effective conductivities of both the solid matrix and solution phase. Tang *et al.*

* Corresponding author at: Eindhoven University of Technology, Eindhoven 5600 MB, the Netherlands.
E-mail address: p.h.l.notten@tue.nl (P.H.L. Notten).
[1] These authors contributed equally to this work.

https://doi.org/10.1016/j.elecom.2020.106865
Received 17 September 2020; Received in revised form 22 October 2020; Accepted 3 November 2020
Available online 6 November 2020

[26] numerically investigated the various values of these effective conductivities.

In the present work, the charge-transfer reaction rate and current distribution across the porous electrodes are analytically derived, and explicit closed-form solutions are obtained, considering a linear approximation of the Butler-Volmer expression at low overpotentials and short-time interval. With this analytical solution, it was possible to study the separate effects of the effective conductivities of solid electrode matrixes and electrolytes on the reaction rate and current distribution inside porous electrodes. When studying these dependencies, four interesting limiting cases are discerned. These analyses are highly useful for further optimizing the electrolyte and electrode properties of LIB and as interesting limiting cases for testing battery modeling software.

2. Model development

To reduce battery modeling complexity, a single porous electrode system has been adopted in the present work. Fig. 1 presents the layout of a C-based porous electrode/Li cell which includes a Li metal foil, a separator membrane and a C-based porous electrode filled with electrolyte. The larger gray solid circles denote the electrode active particles, and the smaller black circles the conducting additives. δ represents the thickness of the separator membrane, and L is the thickness of the whole cell. The thickness of the C-based porous electrode is equal to $L-\delta$. The Li metal/separator interface is defined at $x = 0$, the separator/C-based porous electrode interface at $x = \delta$ and the C-based electrode/current collector interface at $x = L$. The governing equations used to describe the pseudo two-dimensional (P2D) model are summarized in Table S2, where the various physical and electrochemical processes occurring in this specific LIB are listed.

Consider the cell kept in equilibrium, such that no concentration gradients are present and no currents are flowing. Then, at $t = 0$ the constant current density I is applied. The question is how to determine the reaction rate distribution inside the porous C-based electrode at the first moment of current applied. Since there are no concentration gradients, all derivatives related to Li concentration gradients in both the electrode and electrolyte are absent. The system of equations can then be written as

$$i_1 = -\sigma_C \frac{d\,\Phi_1}{dx}, \quad i_1(\delta) = 0, \quad i_1(L) = L, \tag{1}$$

$$i_2 = -\kappa_C \frac{d\,\Phi_2}{dx}, \quad i_2(\delta) = I, \quad i_2(L) = 0, \tag{2}$$

$$\frac{di_2}{dx} = a\ Fj_C = a\, i_C^0 \left[exp\left(\frac{\alpha F\eta_C^{ct}}{RT}\right) - exp\left(-\frac{(1-\alpha)F\eta_C^{ct}}{RT}\right)\right], \tag{3}$$

$$\eta_C^{ct} = \Phi_1 - \Phi_2 - U_C\left(c_1^s, T\right), \tag{4}$$

$$i_1 + i_2 = I. \tag{5}$$

where i_1 and Φ_1 represent the electronic current density ($A\cdot m^{-2}$) and electrical potential (V) in the porous electrode, i_2 and Φ_2 are the ionic current density ($A\cdot m^{-2}$) and electrical potential (V) in the electrolyte inside the porous electrode. Note that subscripts 1 and 2 represent the properties of the electrode and electrolyte, respectively. σ_C and κ_C denote the effective electronic conductivity of the electrode and the effective ionic conductivity of the electrolyte ($S\cdot m^{-1}$), respectively. The effective conductivities account for the actual moving pathways of species in the porous media, for which more detailed information can be found in literature [24,25]. a is the pores specific area (m^{-1}), j_C the reaction rate ($mol\cdot m^{-2}\cdot s^{-1}$), and i_C^0 is the exchange current density ($A\cdot m^{-2}$). Note that j_C becomes current density when multiplied by the Faraday constant F ($C\cdot mol^{-1}$). η_C^{ct} is the charge-transfer overpotential (V), U_C the equilibrium potential of the electrode (V), c_1^s the Li concentration at the electrode particle surface ($mol\cdot m^{-3}$) with space-dependence, I the applied current density ($A\cdot m^{-2}$), and R and T the universal gas constant ($J\cdot mol^{-1}K^{-1}$) and absolute temperature (K), respectively.

Suppose that the current density (I) is applied, and the consequent overvoltage is sufficiently small so that the Butler-Volmer equation can be reduced to a linear relationship according to

$$j_C = \frac{i_C^0}{F}\left[exp\left(\frac{\alpha F\eta_C^{ct}}{RT}\right) - exp\left(-\frac{(1-\alpha)F\eta_C^{ct}}{RT}\right)\right] \approx \frac{i_C^0\eta_C^{ct}}{RT} = \frac{\eta_C^{ct}}{\rho}, \tag{6}$$

where $\rho = \frac{RT}{i_C^0}$.

Then the system of equations simplifies to

$$i_1 = -\sigma_C \frac{d\Phi_1}{dx}, \quad i_1(\delta) = 0, \quad i_1(L) = I, \tag{7}$$

$$i_2 = -\kappa_C \frac{d\,\Phi_2}{dx}, \quad i_2(\delta) = I, \quad i_2(L) = 0, \tag{8}$$

$$\frac{di_2}{dx} = Fa\eta_C^{ct}/\rho = \frac{Fa}{\rho}\left(\Phi_1 - \Phi_2 - U_C\left(c_1^s, T\right)\right), \tag{9}$$

$$i_1 + i_2 = I. \tag{10}$$

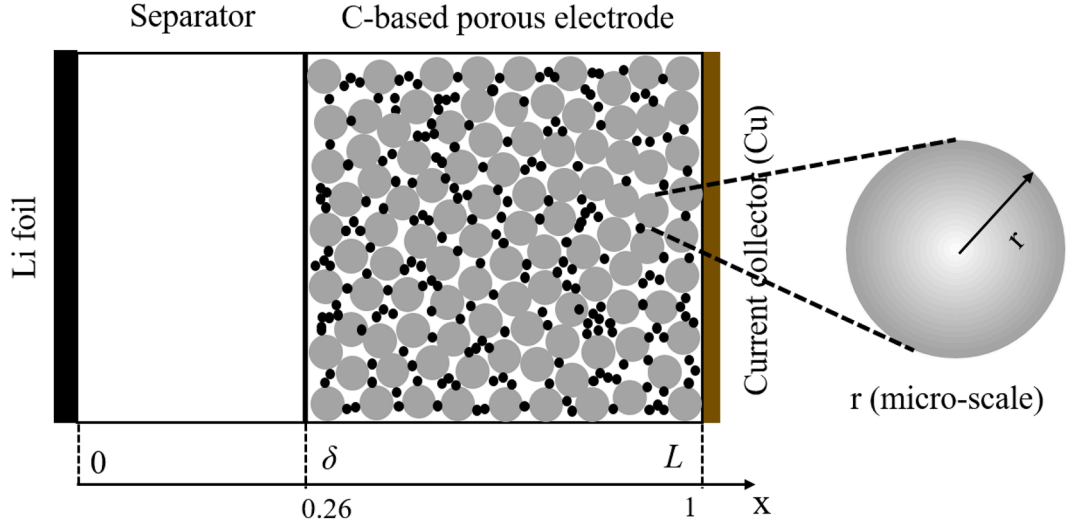

Fig. 1. The layout of a P2D model for a C-based porous electrode/Li cell.

Differentiating Eq. (9) and substituting the derivatives of Φ_1 and Φ_2, by using Eqs. (7) and (8), leads to

$$\frac{d^2 i_2}{dx^2} = \frac{Fa}{\rho}\left(\frac{d\Phi_1}{dx} - \frac{d\Phi_2}{dx}\right) = \frac{Fa}{\rho}\left(-\frac{i_1}{\sigma_C} + \frac{i_2}{\kappa_C}\right). \tag{11}$$

Note that the derivative of $U_C(c_1^s, T)$ vanishes because Li concentrations at the solid surface are constant at the beginning of applying a current. Eliminating i_1 with Eq. (10) gives

$$\frac{d^2 i_2}{dx^2} = \frac{Fa}{\rho}\left(\frac{i_2}{\kappa_C} - \frac{I - i_2}{\sigma_C}\right), \quad i_2(\delta) = I, \quad i_2(L) = 0. \tag{12}$$

Rewriting the right-hand side of Eq. (12) to obtain homogeneous ordinary differential equation (ODE) yields

$$\frac{Fa}{\rho}\left(\frac{i_2}{\kappa_C} - \frac{I - i_2}{\sigma_C}\right) = \frac{Fa}{\rho}\left\{\left(\frac{1}{\kappa_C} + \frac{1}{\sigma_C}\right) i_2 - \frac{I}{\sigma_C}\right\} = \frac{Fa}{\rho}\left(\frac{1}{\kappa_C} + \frac{1}{\sigma_C}\right) i_2^*, \tag{13}$$

where

$$i_2^* = i_2 - I\gamma, \text{ and } \gamma = \frac{1/\sigma_C}{1/\kappa_C + 1/\sigma_C}. \tag{14}$$

Using these new definitions, Eq. (12) is reduced to the following boundary value problem

$$\frac{d^2 i_2^*}{dx^2} = g^2 i_2^*, \quad i_2^*(\delta) = I(1-\gamma), \quad i_2^*(L) = -I\gamma, \tag{15}$$

where $g = \sqrt{\frac{Fa}{\rho}\left(\frac{1}{\kappa_C} + \frac{1}{\sigma_C}\right)}$,

which has a solution of the following form

$$i_2^*(x) = I\frac{\gamma sinh(g(\delta - x)) + (1-\gamma) sinh(g(L-x))}{sinh(g(L-\delta))}, \tag{16}$$

where $sinh(y) = \frac{e^y - e^{-y}}{2}$. Consequently, the solution of Eq. (12) can be written as

$$i_2(x) = I\gamma + i_2^*(x) = I\left(\gamma + \frac{\gamma sinh(g(\delta - x)) + (1-\gamma) sinh(g(L-x))}{sinh(g(L-\delta))}\right), \tag{17}$$

Considering Eq. (3) leads to the following expression for the charge-transfer reaction rate

$$j_C(x) = \frac{1}{Fa}\frac{di_2}{dx} = -\frac{Ig}{Fa}\frac{\gamma cosh(g(\delta - x)) + (1-\gamma) cosh(g(L-x))}{sinh(g(L-\delta))}, \tag{18}$$

where $cosh(y) = \frac{e^y + e^{-y}}{2}$. After back-substitutions of γ and g (Eqs. (14) and (15)), the reaction rate distribution takes its final form

$$j_C(x) = -I\sqrt{\frac{1}{Fa\rho}\left(\frac{1}{\kappa_C} + \frac{1}{\sigma_C}\right)}\frac{\frac{1/\sigma_C}{1/\kappa_C + 1/\sigma_C} cosh\left(\sqrt{\frac{Fa}{\rho}\left(\frac{1}{\kappa_C} + \frac{1}{\sigma_C}\right)}(\delta - x)\right) + \frac{1/\kappa_C}{1/\kappa_C + 1/\sigma_C} cosh\left(\sqrt{\frac{Fa}{\rho}\left(\frac{1}{\kappa_C} + \frac{1}{\sigma_C}\right)}(L - x)\right)}{sinh\left(\sqrt{\frac{Fa}{\rho}\left(\frac{1}{\kappa_C} + \frac{1}{\sigma_C}\right)}(L - \delta)\right)}. \tag{19}$$

3. Results and discussion

From Eq. (19), it can be concluded that a combination of five material-related parameters essentially determines the charge-transfer reaction rate: the thickness of the porous electrode ($L - \delta$), the effective ionic conductivity of the electrolyte inside the porous electrode (κ_C), the effective electronic conductivity of the porous electrode (σ_C), the scaling multiplier $\sqrt{\frac{Fa}{\rho}\left(\frac{1}{\kappa_C} + \frac{1}{\sigma_C}\right)}$ and the (rescaled) flux related to applied current density ($I\sqrt{\frac{1}{Fa\rho}\left(\frac{1}{\kappa_C} + \frac{1}{\sigma_C}\right)}$). Eq. (19) shows that the reaction rate is a weighted sum of two positive terms proportional either to $\frac{1/\sigma_C}{1/\kappa_C + 1/\sigma_C}$ or $\frac{1/\kappa_C}{1/\kappa_C + 1/\sigma_C}$. The first term of Eq. (19) is a monotonically increasing function of x, and the second term is monotonically decreasing.

Table 1
Parameter values used in the simulations.

Parameters	Values	Units
a	$2.0455 \cdot 10^5$	m^{-1}
i_C^0	0.6328	$A \cdot m^{-2}$
R	8.314	$J \cdot mol^{-1} \cdot K^{-1}$
T	298	K
F	96,500	$C \cdot mol^{-1}$
δ	$25 \cdot 10^{-6}$	m
L	$95 \cdot 10^{-6}$	m
I	−9	$A \cdot m^{-2}$
σ_C	10^{-4}–10^{-1}	$S \cdot m^{-1}$
κ_C	10^{-4}–10^{-1}	$S \cdot m^{-1}$

The next two figures illustrate the dependencies of the reaction rate distribution and the ionic current in the electrolyte on the effective electronic and ionic conductivities (κ_C and σ_C) for a set of parameter values given in Table 1, where a and i_C^0 are the optimized values inferred from experimental data described elsewhere [27], δ and L are measured values, I is the applied current density (approximately 0.2C, 1C = 45 $A \cdot m^{-2}$), and T is the temperature at which all simulations are performed. Figs. 2 and 3 are obtained by simulating Eqs. (19) and (17), using MATLAB R2018b as the software. Fig. 2 shows the simulated reaction rate profiles $j_C(x)$ across the electrode thickness as a function of κ_C and σ_C, keeping the other parameters as listed in Table 1. Fig. 2a explains the choices of the parameters used in the subsequent plots. The colored lines marked by letters (b–f) in Fig. 2a indicate the parameters selection in Fig. 2b–f, respectively. Each line represents a subset of parameters κ_C and σ_C used to show the corresponding surface plot. The conductivities are effective conductivities and are in the range of 10^{-4} to 10^{-1} $S \cdot m^{-1}$. If the porosity of the porous electrode (ε) is equal to 0.25 and the Bruggeman coefficient ($Brugg$) is 2, then according to the relation $\kappa_C = \kappa\ \varepsilon^{Brugg}$, the electrode and electrolyte conductivities range of $1.6 \cdot 10^{-3}$ to 1.6 $S \cdot m^{-1}$. In Fig. 2b, the reaction rate $j_C(x)$ inside the porous electrode is plotted from the normalized position $x = 0.26$ onwards to $x = 1$ for the case where $\kappa_C = \sigma_C$. It can be seen that in this specific case, the reaction rate is symmetric with respect to the electrode mid-point ($x = (L + \delta)/2$). When both κ_C and σ_C are very small, the reaction rate dominates at the two interfaces at $x = 0.26$ and $x = 1$. When both conductivities start to increase, the reaction rate starts to move inside the porous electrode, while its values at both interfaces are decreasing. When both κ_C and σ_C are large, for example, 0.1 $S \cdot m^{-1}$ or

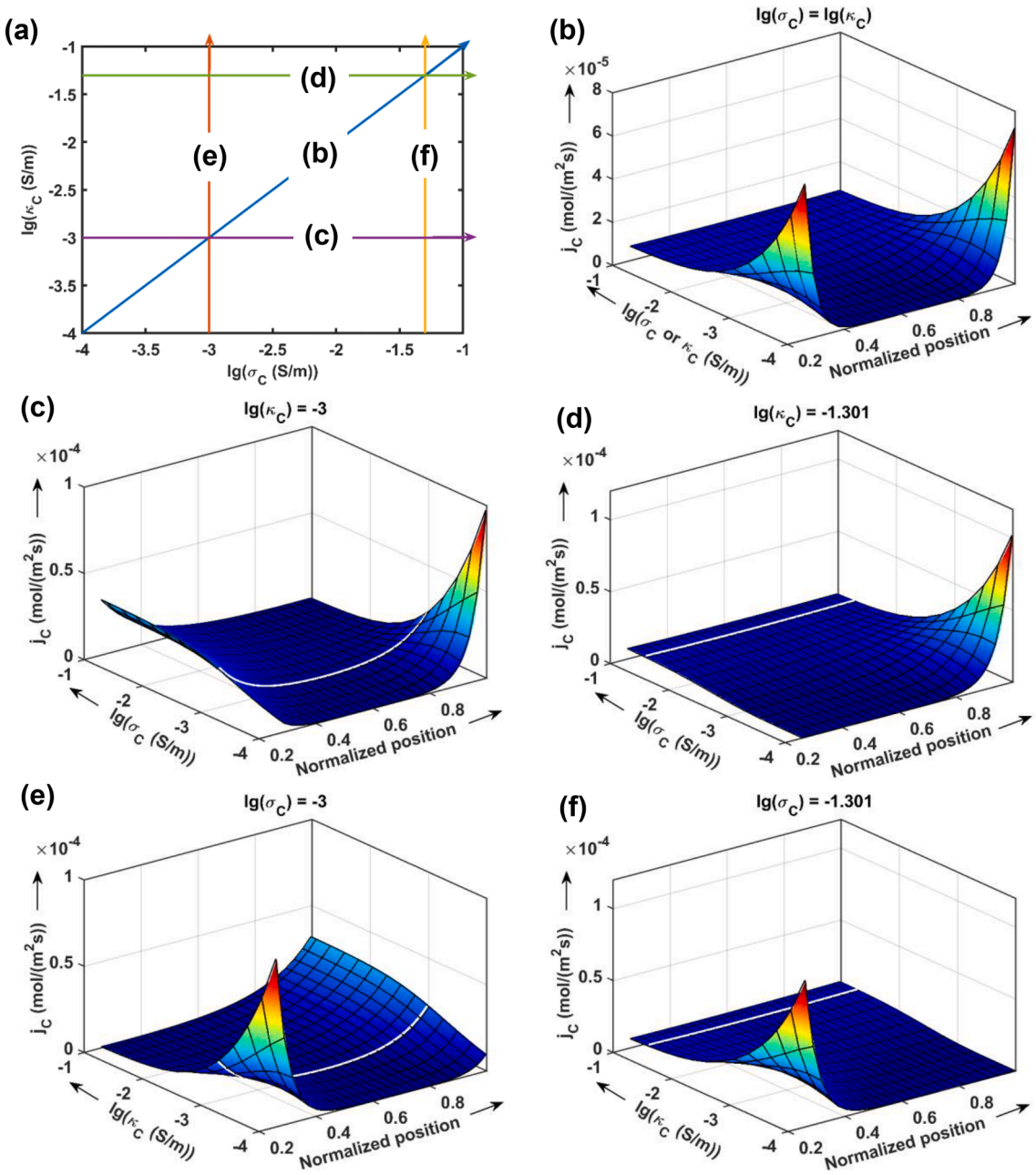

Fig. 2. Reaction rate distribution (j_C) as a function of normalized position x inside the porous electrode, κ_C and σ_C. (a) Selections of value ranges of κ_C and σ_C in (b-f). (b) Symmetric case $\sigma_C = \kappa_C$. Dependence on σ_C for (c) $\kappa_C = 0.001$ S·m^{-1} and (d) $\kappa_C = 0.05$ S·m^{-1}. Dependence on κ_C for (e) $\sigma_C = 0.001$ S·m^{-1} and (f) $\sigma_C = 0.05$ S·m^{-1}.

above, j_C is close to uniform.

Fig. 2c and d show the dependence of $j_C(x)$ on σ_C for two cases when κ_C has a negligibly small value of 0.001 S·m^{-1} (c), or has a moderate value of 0.05 S·m^{-1} (d). When the effective electronic conductivity σ_C increases from small to large values, the dominant reaction rate at the electrode/current collector interface ($x = 1$) starts to decrease to finally disappear in both cases. It can be seen that a small value of κ_C makes the reaction rate more dominant at the electrode/separator interface at $x = 0.26$ when σ_C becomes large (Fig. 2c). For a moderate value of κ_C such a prominent effect is absent (Fig. 2d).

Fig. 2e and f show the dependence of $j_C(x)$ on κ_C when σ_C is either small at 0.001 S·m^{-1} (e) or has a moderate value of 0.05 S·m^{-1} (f). When κ_C increases, the dominant effect of reaction rate at the electrode/separator interface at $x = 0.26$ starts to decrease and finally disappears in both cases. The small value of σ_C makes the reaction rate more dominant at the electrode/current collector interface at $x = 1$ when κ_C becomes large (Fig. 2e). A moderate value of σ_C does not show such an effect (Fig. 2f). Apparently, Fig. 2e and f mirror Fig. 2c and d flipped around the mid-point of the electrode. In all four figures (c-f) the thin white lines correspond to a situation where κ_C and σ_C are equal. Thus the white lines represent all the symmetric cases with respect to the electrode mid-point.

Fig. 3 shows the ionic current profiles $i_2(x)$ in the electrolyte along with the electrode thickness as a function of parameters κ_C and σ_C. The relationship between $i_2(x)$ and $j_C(x)$ in the porous electrode is given by Eq. (18). Essentially, the reaction rate $j_C(x)$ is the re-normalized derivative of $i_2(x)$. Fig. 3a illustrates the parameter choices used in the subsequent plots, similar to Fig. 2a. Fig. 3b shows the specific case that $\kappa_C = \sigma_C$. When both κ_C and σ_C are small, the ionic current has sharp increases at both interfaces and a well-defined flat part in between. This

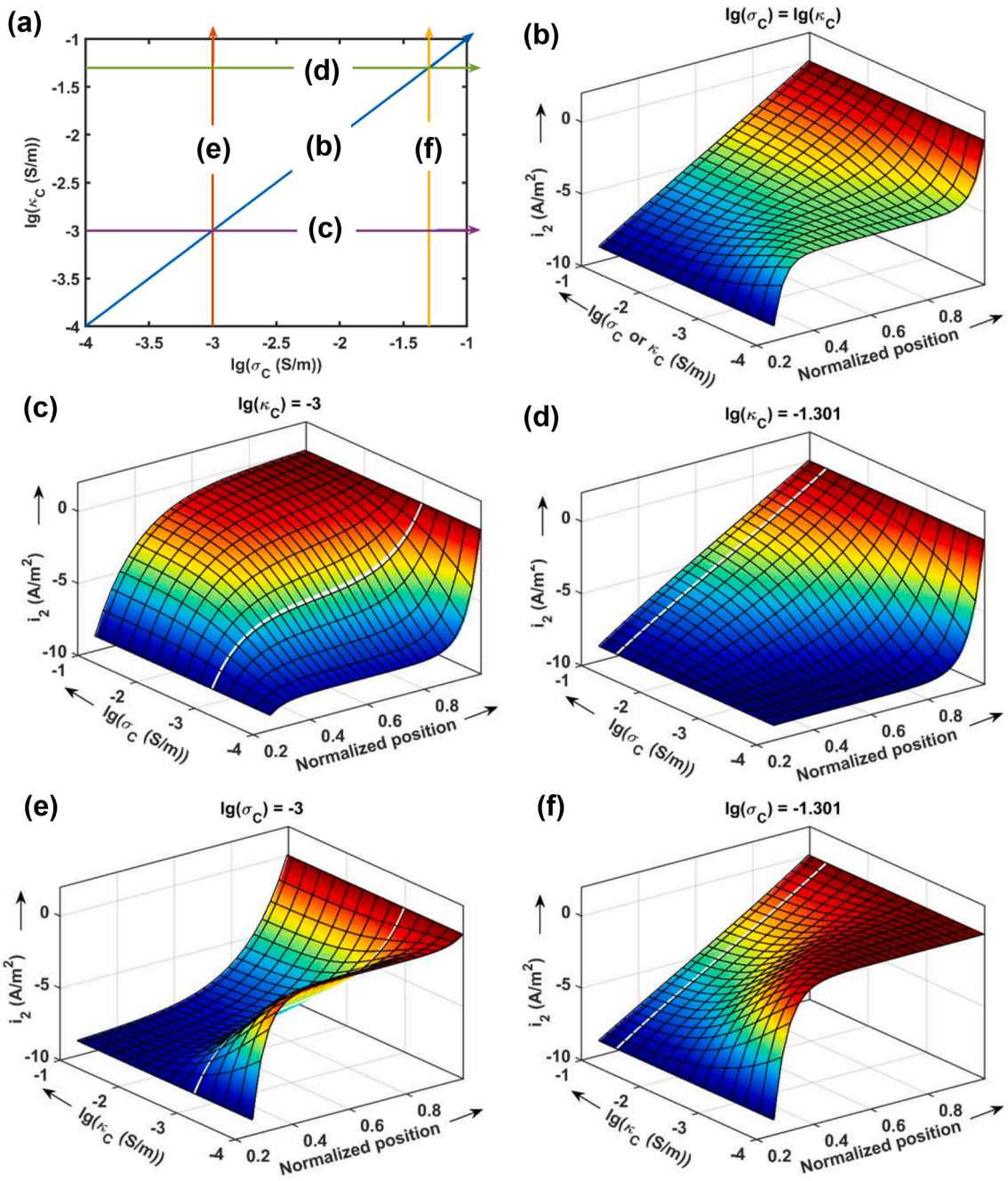

Fig. 3. Ionic current density inside the porous electrode (i_2) as a function of κ_C and σ_C. (a) Selections of value ranges of κ_C and σ_C in (b-f). (b) Symmetric case $\sigma_C = \kappa_C$. Dependence on σ_C for (c) $\kappa_C = 0.001$ S·m^{-1} and (d) $\kappa_C = 0.05$ S·m^{-1}. Dependence on κ_C for (e) $\sigma_C = 0.001$ S·m^{-1} and (f) $\sigma_C = 0.05$ S·m^{-1}.

dependence is symmetric with respect to the electrode mid-point and can be called inverse sigmoidal. When both κ_C and σ_C increase, the ionic current converges to a linear function at 0.1 S·m^{-1}.

Fig. 3c and d show the dependence of the ionic current profile on σ_C, when κ_C is either 0.001 (c) or 0.05 S·m^{-1} (d). Fig. 3c shows that in the case of a small value of κ_C, increasing σ_C transforms the shape of $i_2(x)$ from inverse sigmoidal to concave, with a sharp increase near the electrode/separator interface at $x = 0.26$. In contrast, in the case of a more moderate value for κ_C (Fig. 3d), increasing σ_C changes the profile from convex with a sharp increase near the electrode/current collector interface at $x = 1$ to linear dependence. Fig. 3e and f show the dependence of $i_2(x)$ on κ_C when σ_C is changing from 0.001 (e) to 0.05 S·m^{-1} (f). Fig. 3e shows that small values of σ_C and κ_C lead to a concave shape with sharp increases near the electrode/separator interface at $x = 0.26$. When κ_C grows, $i_2(x)$ converges to the convex limiting function with an apparent increase near the electrode/current collector interface at $x = 1$. Fig. 3f shows how the concave limiting distribution with a sharp increase at the electrode/separator interface at x = 0.26 and almost constant values inside the electrode transforms into a linear dependence at large values of κ_C. The thin white lines in Fig. 3c-f correspond to cases where κ_C and σ_C are equal, similar to Fig. 2c–f.

The main conclusion from Figs. 2 and 3 is that both the ionic and electronic conductivities are essential for the reaction rate distribution and ionic current density distribution inside porous electrodes. Small values of κ_C cause the reaction rate to become dominant at the electrode/separator interface (Fig. 2f), while small values of σ_C make the reaction rate more intense at the electrode/current collector interface (Fig. 2d). When both κ_C and σ_C are small, the reaction rate will be

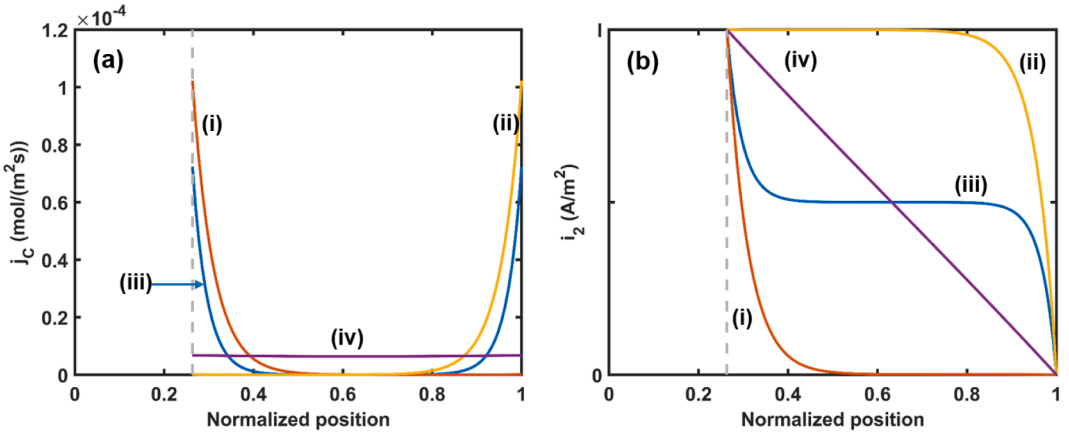

Fig. 4. Four limiting cases can be distinguished for the reaction rate distribution j_C (a) and the ionic current distribution i_2 (b). Case (*i*) corresponds to a low effective ionic conductivity ($\kappa_C << \kappa_{sat}$), but good effective electronic conductivity ($\sigma_C \geqslant \sigma_{sat}$); case (*ii*) holds for the opposite condition, a low effective electronic conductivity is combined with a good effective ionic conductivity ($\kappa_C \geqslant \kappa_{sat}$ and $\sigma_C << \sigma_{sat}$); case (*iii*) describes a situation when both effective conductivities are low ($\kappa_C << \kappa_{sat}$ and $\sigma_C << \sigma_{sat}$); case (*iv*) corresponds to the situation when both effective conductivities are high ($\kappa_C \geqslant \kappa_{sat}$ and $\sigma_C \geqslant \sigma_{sat}$).

dominant at both interfaces (Fig. 2b, c, and e).

Interesting features can be observed when studying Figs. 2 and 3 in more detail. When the values of κ_C and σ_C increase above a certain saturation value, denoted as κ_{sat} and σ_{sat}, the $j_C(x)$ and $i_2(x)$ functions are not changing anymore (see Supporting Information for a more detailed explanation). The saturation values κ_{sat} and σ_{sat} are defined as

$$\frac{1}{\kappa_{sat}} = \frac{1}{\sigma_{sat}} = \frac{\beta^2 \rho}{2(L-\delta)^2 Fa} = \frac{\beta^2 RT}{2(L-\delta)^2 Fa\, i_C^0}, \tag{20}$$

where β denotes a saturation level, which makes $cosh(\beta)$ become close to 1. For example, if $cosh(\beta) = 1.01$, *i.e.* 1% larger than 1, then $\beta = cosh^{-1}(1.01) = 0.1413$. From Eq. (20) κ_{sat} and σ_{sat} are directly proportional to the (squared) thickness $(L-\delta)$, the specific area (a) of the porous electrode, and the exchange current density (i_C^0) of the charge-transfer reaction, and other constants R^{-1}, T^{-1}, F. Fig. S2 in the Supporting Information illustrates the reaction rate distribution with larger exchange current density, thicker electrode, or larger specific area when all other parameters kept the same as used for the simulations shown in Figs. 2 and 3.

To explain the potential use of saturation values, two examples are presented here. The electrolyte generally used in LIB has an ionic conductivity in the range of 0 to 1 $S \cdot m^{-1}$, depending on the electrolyte concentration and temperature [28,29]. The electronic conductivity of $LiFePO_4$ (LFP) particles is generally as low as $\sim 10^{-7}\, S \cdot m^{-1}$ [30,31]. The effective electronic and ionic conductivities in the porous electrode need to be further modified considering the electrode porosity (ε) and Bruggeman coefficient (*Brugg*), leading to even smaller values. When no conductive coatings are deposited onto the LFP particles and no conductive additives are introduced in the porous electrodes, the low effective electronic conductivity of the LFP electrode and comparative large effective ionic conductivity will make the reaction rate dominant near the electrode/current collector interface. Increasing the effective electronic conductivity by coating conductive material on the surface of the LFP particles or adding conductive additives to the electrode will be a good solution to alleviate the inhomogeneity of the reaction rate distribution. However, if after such an improvement the effective conductivity of a porous LFP electrode is already beyond σ_{sat}, a further increase in electronic conductivity will no longer be of any help to increase the homogeneity of the reaction rate distribution. Optimization of the battery performance by reducing the thickness of the porous electrode, reducing the particle size or modifying the electrode/electrolyte interface will be more helpful in this situation.

For graphite electrodes, considering conducting additives and a well-developed porous microstructure, a high effective electronic conductivity and a low effective ionic conductivity (values smaller than κ_{sat}) induce the reaction rate distribution to become dominant near the separator/electrode interface. Increasing the effective ionic conductivity or decreasing κ_{sat} will make the reaction rate distribution more uniform across the porous electrode.

In general, the smaller values of the effective conductivities than the saturation values will make the reaction rate even more non-uniform. Increasing only the electrode thickness [32] will increase the saturation values κ_{sat} and σ_{sat}. Increasing the tortuosity while keeping the porosity the same [33] will decrease the effective conductivities but do not change κ_{sat} and σ_{sat}. In these two cases, the reaction rate will become even more dominant near the separator/electrode interface because the effective ionic conductivity deviates more from κ_{sat} considering a large effective electronic conductivity. Changing the porosity in various ways could lead to various conclusions. Decreasing the porosity without changing the specific area [34] can only reduce the effective conductivities with the same saturation values. Decreasing the porosity by changing particle size of the electroactive material [34] will also change the saturation values. In the latter case, the effective conductivities need to be calculated and compared with the changed saturation values to decide the reaction rate distribution.

The inaccuracy of the linear approximation for the Butler-Volmer equation at low overpotentials is another interesting question to also address here. A comparison between the Butler-Volmer equation and the linear approximated relationship is presented in Fig. S3. If a 10% error is permitted, then the overpotential-current relation in the range of −41 to 41 mV can be considered linear ($\alpha = 0.5$), and the overpotential of 41 mV is corresponding to the current density of 0.36C.

Finally, concerning the value variations of κ_C and σ_C, it is worthwhile to mention that all limiting cases of the reaction rate and current density distribution can be classified into four basic types. Fig. 4 shows these 4 cases where case (*i*) corresponds to a poor effective ionic and moderate effective electronic conductivities; case (*ii*) holds for the opposite case, low effective electronic and moderate effective ionic conductivity; case (*iii*) describes the situation when both effective conductivities are low, and case (*iv*) corresponds to the situation when both effective conductivities are high.

4. Conclusions

An interesting specific case of porous electrode modeling is considered, describing a rechargeable battery with a single porous electrode and a non-porous metallic lithium electrode. The reaction rate distribution inside the porous electrode is mathematically derived for short

moment after switching on the current. Applying a linear approximation to the Butler-Volmer equation at low overpotentials leads to an analytical solution of a relatively simple form (Eq. (19)). In contrast to the case of the Tafel approximation [14] or asymptotic solution [16], the reaction distribution depends on both the effective electronic and ionic conductivities (σ_C and κ_C). From the analyses, it has been concluded that four limiting cases can be discerned for the reaction rate and ionic current distribution, as summarized in Fig. 4. The present results are essential for further optimizing the electrolyte and electrode properties and can easily be generalized to conventional batteries using two porous electrodes.

CRediT authorship contribution statement

Zhiqiang Chen: Conceptualization, Software, Validation, Writing - original draft. **Dmitri L. Danilov:** Conceptualization, Methodology, Software, Supervision, Writing - original draft. **Rüdiger-A. Eichel:** Project administration. **Peter H.L. Notten:** Conceptualization, Supervision, Writing - review & editing.

Declaration of Competing Interest

The authors declare that they have no known competing financial interests or personal relationships that could have appeared to influence the work reported in this paper.

Acknowledgement

Zhiqiang Chen gratefully acknowledges fellowship support by the China Scholarship Council.

Appendix A. Supplementary data

Supplementary data to this article can be found online at https://doi.org/10.1016/j.elecom.2020.106865.

References

[1] J. Han, H. Li, D. Kong, C. Zhang, Y. Tao, H. Li, Q.-H. Yang, L. Chen, ACS Energy Lett. 5 (2020) 1986–1995.
[2] Z. Chen, J.R. Dahn, J. Electrochem. Soc. 149 (2002) A1184–A1189.
[3] X. Lou, Y. Zhang, J. Mater. Chem. 21 (2011) 4156–4160.
[4] M. Singh, J. Kaiser, H. Hahn, J. Electrochem. Soc. 162 (2015) A1196–A1201.
[5] H. Zheng, J. Li, X. Song, G. Liu, V.S. Battaglia, Electrochim. Acta 71 (2012) 258–265.
[6] R. Zhao, J. Liu, J. Gu, Appl. Energy 139 (2015) 220–229.
[7] Z. Du, D.L. Wood, C. Daniel, S. Kalnaus, J. Li, J. Appl. Electrochem. 47 (2017) 405–415.
[8] Y. Zhang, Z. Yang, C. Tian, J. Mater. Chem. A 7 (2019) 23628–23661.
[9] H. Murayama, K. Kitada, K. Fukuda, A. Mitsui, K. Ohara, H. Arai, Y. Uchimoto, Z. Ogumi, E. Matsubara, J. Phys. Chem. C 118 (2014) 20750–20755.
[10] S.J. Harris, A. Timmons, D.R. Baker, C. Monroe, Chem. Phys. Lett. 485 (2010) 265–274.
[11] H. Tanida, H. Yamashige, Y. Orikasa, Y. Gogyo, H. Arai, Y. Uchimoto, Z. Ogumi, J. Phys. Chem. C 120 (2016) 4739–4743.
[12] Z. Nie, P. McCormack, H.Z. Bilheux, J.C. Bilheux, J.P. Robinson, J. Nanda, G. M. Koenig, J. Power Sources 419 (2019) 127–136.
[13] J. Nanda, H. Bilheux, S. Voisin, G.M. Veith, R. Archibald, L. Walker, S. Allu, N. J. Dudney, S. Pannala, J. Phys. Chem. C 116 (2012) 8401–8408.
[14] F. Rittweger, C. Modrzynski, V. Roscher, D.L. Danilov, P.H.L. Notten, K.-R. Riemschneider, J. Power Sources 482 (2021), 228943.
[15] Y. Orikasa, Y. Gogyo, H. Yamashige, M. Katayama, K. Chen, T. Mori, K. Yamamoto, T. Masese, Y. Inada, T. Ohta, Z. Siroma, S. Kato, H. Kinoshita, H. Arai, Z. Ogumi, Y. Uchimoto, Sci. Rep. 6 (2016) 26382.
[16] G. Inoue, M. Kawase, J. Power Sources 342 (2017) 476–488.
[17] J. Newman, C.W. Tobias, J. Electrochem. Soc. 109 (1962) 1183–1191.
[18] J. Newman, W. Tiedemann, AIChE J. 21 (1975) 25–41.
[19] R. Darling, J. Newman, J. Electrochem. Soc. 144 (1997) 3057–3063.
[20] K. Scott, P. Argyropoulos, J. Electroanal. Chem. 567 (2004) 103–109.
[21] O. Lanzi, U. Londou, J. Electrochem. Soc. 137 (1990) 585–593.
[22] S.S.T. Katan, J. Electrochem. Soc. 122 (1975) 1063–1071.
[23] R.J. Brodd, Electrochim. Acta 11 (1966) 1107–1117.
[24] M. Doyle, T.F. Fuller, J. Newman, J. Electrochem. Soc. 140 (1993) 1526–1533.
[25] T.F. Fuller, M. Doyle, J. Newman, J. Electrochem. Soc. 141 (1994) 1–10.
[26] Y. Tang, M. Jia, J. Li, Y. Lai, Y. Cheng, Y. Liu, J. Electrochem. Soc. 161 (2014) E3021–E3027.
[27] Z. Chen, D.L. Danilov, K. Chayambuka, L. Zhou, M. Jiang, L.H.J. Raijmakers, J. Zhou, R.-A. Eichel, P.H.L. Notten, submitted to Electrochim. Acta, (2020).
[28] L.O. Valoen, J.N. Reimers, J. Electrochem. Soc. 152 (2005) A882–A891.
[29] E. Prada, D. Di Domenico, Y. Creff, J. Bernard, V. Sauvant-Moynot, F. Huet, J. Electrochem. Soc. 159 (2012) A1508–A1519.
[30] C. Wang, J. Hong, Electrochem. Solid-State Lett. 10 (2007) A65–A69.
[31] M.M. Doeff, J.D. Wilcox, R. Kostecki, G. Lau, J. Power Sources 163 (2006) 180–184.
[32] N. Ogihara, Y. Itou, T. Sasaki, Y. Takeuchi, J. Phys. Chem. C 119 (2015) 4612–4619.
[33] J. Landesfeind, A. Eldiven, H.A. Gasteiger, J. Electrochem. Soc. 165 (2018) A1122–A1128.
[34] J. Ye, A.C. Baumgaertel, Y.M. Wang, J. Biener, M.M. Biener, ACS Nano 9 (2015) 2194–2202.